water

MDPI

*Article*

# Experimental Study on Mode I Fracture Characteristics of Granite after Low Temperature Cooling with Liquid Nitrogen

**Linchao Wang [1], Yi Xue [1], Zhengzheng Cao [2,*], Hailing Kong [3], Jianyong Han [4] and Zhizhen Zhang [5]**

[1] State Key Laboratory of Eco-Hydraulics in Northwest Arid Region, Xi'an University of Technology, Xi'an 710048, China
[2] International Joint Research Laboratory of Henan Province for Underground Space Development and Disaster Prevention, Henan Polytechnic University, Jiaozuo 454000, China
[3] College of Civil Engineering, Yancheng Institute of Technology, Yancheng 224051, China
[4] School of Civil Engineering, Shandong Jianzhu University, Jinan 250101, China
[5] School of Mechanics and Civil Engineering, China University of Mining and Technology, Xuzhou 221116, China
* Correspondence: caozz2008@126.com

**Abstract:** Liquid nitrogen fracturing has emerged as a promising technique in fluid fracturing, providing significant advantages for the utilization and development of geothermal energy. Similarly to hydraulic fracturing in reservoirs, liquid nitrogen fracturing entails a common challenge of fluid–rock interaction, encompassing the permeation and diffusion processes of fluids within rock pores and fractures. Geomechanical analysis plays a crucial role in evaluating the transfer and diffusion capabilities of fluids within rocks, enabling the prediction of fracturing outcomes and fracture network development. This technique is particularly advantageous for facilitating heat exchange with hot dry rocks and inducing fractures within rock formations. The primary objective of this study is to examine the effects of liquid nitrogen fracturing on hot dry rocks, focusing specifically on granite specimens. The experimental design comprises two sets of granite samples to explore the impact of liquid nitrogen cooling cycles on the mode I fracture characteristics, acoustic emission features, and rock burst tendency of granite. By examining the mechanical properties, acoustic emission features, and rock burst tendencies under different cycling conditions, the effectiveness of liquid nitrogen fracturing technology is revealed. The results indicate that: (1) The ultimate load-bearing capacity of the samples gradually decreases with an increase in the number of cycling times. (2) The analysis of acoustic emission signals reveals a progressive increase in the cumulative energy of the samples with cycling times, indicating that cycling stimulates the release of stored energy within the samples. (3) After undergoing various cycling treatments, the granite surface becomes rougher, exhibiting increased porosity and notable mineral particle detachment. These results suggest that the cyclic application of high-temperature heating and liquid nitrogen cooling promotes the formation of internal fractures in granite. This phenomenon is believed to be influenced by the inherent heterogeneity and expansion–contraction of internal particles. Furthermore, a detailed analysis of the morphological sections provides insights into the structural changes induced by liquid nitrogen fracturing in granite samples.

**Keywords:** liquid nitrogen; granite; mechanical properties; morphological sections



**Citation:** Wang, L.; Xue, Y.; Cao, Z.; Kong, H.; Han, J.; Zhang, Z. Experimental Study on Mode I Fracture Characteristics of Granite after Low Temperature Cooling with Liquid Nitrogen. *Water* **2023**, *15*, 3442. https://doi.org/10.3390/w15193442

Academic Editor: Helena M. Ramos

Received: 25 August 2023
Revised: 26 September 2023
Accepted: 27 September 2023
Published: 30 September 2023



## 1. Introduction

Fluids play a fundamental role in linking the lithosphere, atmosphere, and biosphere, facilitating the exchange of matter and energy within and between these spheres. As formidable geological agents, they profoundly shape diverse geologic processes and intricate ecological–environmental dynamics [1]. In order to investigate the mechanical properties of cryogenically treated rocks, this study focuses on the complex interactions between fluids and rocks. Specifically, the process of liquid nitrogen fracturing involves injecting high-pressure liquid nitrogen into rock fissures, allowing the fluid to establish contact with both the rock surface and internal structure. This intricate process encompasses the permeation and diffusion of fluids within the porous network and fractures of the rock [2,3]. The introduction of liquid nitrogen subsequently induces considerable pressure, significantly altering the deformation and stress-distribution characteristics of the rock. In addition, the remarkably low temperature of liquid nitrogen elicits prominent thermal variations upon contact with the rock, triggering notable thermal expansion and contraction effects [4]. These phenomena intricately influence the physical properties and mechanical response of the rock. Notably, the liquid nitrogen fracturing process facilitates material exchanges between the fluid and rock, encompassing essential mechanisms, such as dissolution, adsorption, and chemical reactions.

In conclusion, geomechanical analyses of fluid–rock interactions allow us to assess the intricate transmission and diffusion capabilities of fluids within rocks, enabling the prediction of fracturing outcomes and the evolution of fracture networks [5,6]. By investigating the elastic and plastic behavior of rocks, we can anticipate the probabilities of rock rupture and slippage, facilitating the evaluation of the impact of liquid nitrogen fracturing techniques on rock formations. Understanding the ramifications of temperature fluctuations on factors such as rock strength, crack propagation, and stress dissipation is of utmost importance. By exploring the intricate mechanisms governing the exchange of mate-rials between rocks and fluids, and simultaneously evaluating the influences of liquid nitrogen fracturing techniques on reservoir characteristics and chemical environments, we can establish a comprehensive understanding of the efficacy and underlying mechanisms associated with liquid nitrogen fracturing in rock formations.

Recently, emerging resources such as geothermal energy have gradually become strategic alternatives in the field of renewable energy. Geothermal resources encompass various types, including shallow geothermal energy, hydrothermal geothermal resources, and hot dry rock resources [7]. Currently, the available geothermal resources mainly con-sist of shallow geothermal energy extracted using heat pump technology, geothermal flu-ids acquired through artificial drilling, and geothermal resources located in hot dry rock formations. However, extracting resources from hot dry rocks can be challenging due to their relatively low natural permeability. Establishing effective flow channels and fracturing hot dry rock reservoirs is an essential concern in developing and utilizing geothermal energy. Various techniques are employed for fracturing, including hydraulic fracturing, thermal stimulation, and chemical stimulation [8–10]. Among these methods, hydraulic fracturing has proven to be the most commonly used and effective technique in practical engineering, particularly in the oil and gas exploration industry. However, in practical applications, hydraulic fracturing often leads to the formation of a single large fracture in hot dry rocks, reducing the heat exchange area, which contradicts the original intention of enhanced geothermal systems (EGS) engineering [11]. In this context, liquid nitrogen fracturing technology has once again attracted people's attention, as the low-temperature characteristics of liquid nitrogen fluids can effectively reduce the fracture pressure of high-temperature rocks [12,13].

Numerous scholars have conducted extensive research on liquid nitrogen fracturing in rocks. King et al. [14] conducted fracturing experiments on dry sandstone reservoirs using low-temperature liquid carbon dioxide. Their findings indicate that the transition of $CO_2$ from liquid to gas under reservoir conditions does not induce water blockage or clay swelling effects in low-permeability water-sensitive reservoirs. They identified several advantages of low-temperature liquid $CO_2$ fracturing, including a high fluid recovery rate and a reduction in crude oil viscosity. McDaniel et al. [15] observed significant thermal shock on the rock surface when injecting liquid nitrogen into high-temperature rock reservoirs, resulting in crack initiation and propagation. Furthermore, the freezing effect caused by contact between reservoir fluids and liquid nitrogen enhances reservoir permeability. Grundmann et al. [16] successfully conducted liquid nitrogen fracturing operations on shale gas wells using fiberglass steel pipes and stainless-steel wellheads. They applied pressure of 20 MPa and injected 42.3 tons of liquid nitrogen. Cha et al. [17] con-ducted laboratory experiments on low-temperature fracturing and found that increasing the injection volume of liquid nitrogen effectively improves the fracturing effect. They also emphasized the importance of minimizing the Leidenfrost effect to optimize the cooling rate of the rock, as the thermal shock impact strongly correlates with rock lithology. Through techniques such as nuclear magnetic resonance, Cai et al. [18] investigated the impact of liquid nitrogen on the physical properties of coal, sandstone, and shale. Their findings revealed frozen damage and the formation of surface thermal cracks when applying liquid nitrogen. This promotes internal crack propagation and enhances permeability, and the degree of damage increases with higher water content. Han et al. [19] demonstrated that utilizing liquid nitrogen as a pretreatment method significantly enhances the fracturing performance of shale reservoirs, reducing initiation pressure and time by approximately 54% and 60%, respectively. Additionally, liquid nitrogen application increases transformed fracture volume and complexity. Zhang et al. [20,21], through numerical simulations and experimental research, found that liquid nitrogen abrasive jets have a greater impact on high-temperature rocks, resulting in the formation of more complex pores. Yang et al. [22] conducted gas fracturing experiments on granite samples pretreated with liquid nitrogen, which demonstrated a notable impact on the fracturing pressure of the rock samples. In terms of rock fracture toughness, Yin et al. [23] discovered that the fracture toughness of granite significantly decreased with an increase in the number of heating and liquid nitrogen cooling cycles. Thermal shock, thermal stress, and fatigue damage are the main factors contributing to the continuous deterioration of rock mechanical properties [24]. Shao et al. [25] reached a similar conclusion through a three-point bending test on granite cooled with liquid nitrogen and also emphasized the influence of the initial temperature of the granite on mode I fracture characteristics. They found that as the heating temperature increased, the fracture toughness initially increased and then decreased, while the fracture roughness continued to increase. In summary, current research on liquid nitrogen fracturing mainly focuses on low-temperature rocks, and the impact on high-temperature rocks, such as dry hot rocks, remains unclear. Additionally, our understanding of mode I fracture characteristics in granite is limited. Therefore, further research in this field is necessary.

Acoustic emission experiments have been widely utilized in rock mechanics testing worldwide. The primary focus of acoustic emission research is to investigate the characteristics exhibited by rocks, concrete, and coal during uniaxial compression tests and conventional triaxial tests [26]. Additionally, significant attention has been given to studying acoustic emission in laboratory environments, particularly in utilizing this technique to understand the process and mechanism of rock brittle failure. Many scholars have made essential contributions in this area [27–34]. In this study, the impact of multiple heating and liquid nitrogen cooling on the mechanical properties of granite was examined through three-point bending tests. The evolution of mode I fracture characteristics and fracture surface roughness of granite was investigated using acoustic emission systems and 3D profilometry. Furthermore, the damaging and fracturing effects of liquid nitrogen on high-temperature rocks were analyzed.

## 2. Design of Experiments

### *2.1. Preparation of Test Rock Samples*

Taking into consideration the physical properties and distribution characteristics of hot dry rocks, as well as the regional distribution of geothermal resources in China, granite samples from Xuzhou, China were selected as the experimental rock samples for this study. Granite, an elastic igneous rock with minimal porosity and limited permeability [35], bears close resemblance to hot dry rocks in terms of these physical characteristics. Thus, granite serves as an appropriate representative sample for investigating hot dry rocks. The initial rock samples were carefully sealed and transported to the laboratory under secure conditions. In a controlled environment, specialized equipment was employed to process the original rocks, resulting in the acquisition of processed rock samples, as depicted in Figure 1. To mitigate the potential impact of rock heterogeneity on the experimental outcomes, all rock samples were obtained from a single rock block. The rock sample used for the three-point bending test is shown in Figure 2, with a thickness of 30 mm and a diameter of 76 mm. To induce a semicircular crack oriented vertically relative to the bottom diameter, a precise artificial notch measuring 14 mm in length was meticulously introduced. It is important to emphasize that the surface flatness of the rock samples, the width of the precut notch, and the perpendicularity of the precut crack all conform to the tolerance range specified by the International Society for Rock Mechanics (ISRM) [36].

**Figure 1.** Granite specimens.

**Figure 2.** Half-disc sample of granite.

## 2.2. Experimental Equipment

The experiment utilized various equipment, including a heating box, liquid nitrogen tank, non-metallic ultrasonic monitoring analyzer, CSS-44100 testing machine, PCI-2 acoustic emission system, and VR-5000 series 3D profilometer. The sound emission is carried out using the dedicated sound emission system PCI-2 produced by the American Physical Acoustics Corporation (PAC). The non-metallic ultrasonic monitoring analyzer is produced by Beijing Koncrete Testing Technology Co., Ltd. in China, and the 3D profiler is the VR-5000 series 3D profiler produced by a Japanese company. The heating box and liquid nitrogen tank are all conventional instruments produced in China. The non-metallic ultrasonic monitoring analyzer can non-destructively detect the changes in wave velocity inside granite, with an emission voltage of 500 V and a sampling period of 0.4 µs. The CSS-44100 testing machine is an advanced testing system used for studying and testing the mechanical properties of rocks [37]. The CSS-44100 testing machine is produced by

Changchun Machinery Science Research Institute Co., Ltd. in China. In the experiment, axial displacement control was employed at a rate of 0.05 mm/min. The PCI-2 acoustic emission system features an 18-bit A/D converter with a frequency range of 1 kHz to 3 MHz. The preamplifier for acoustic emission was set at 40 dB, with a threshold value of 35 dB. The acoustic emission detection system is equipped with four high-pass and six low-pass filters, which can be selected and controlled through software. During the experiment, the acoustic emission transducer was installed at the middle position of the specimen to monitor and record real-time fracture information of the rock. The VR-5000 series 3D profilometer was used to scan the fracture surface of the rock specimen. This device has a maximum resolution of up to 160X and a zoom range of 1–4 times. To obtain clear scanned images of the rock fracture surface, the scanning magnification was set to 12 times.

### *2.3. Experimental Procedure*

After the preparation of the granite specimens, high-temperature heating and liquid nitrogen cooling experiments were conducted. Initially, the granite specimens were placed inside a heating box with the temperature set to 300 °C. To prevent damage to the rock from rapid heating, the heating rate was controlled at 5 °C/min. The granite was heated up to 300 °C and maintained at this temperature for 3 h to ensure thorough heating of the rock. Following the heating process, the specimens were transferred to a liquid nitrogen tank for cooling, with a cooling duration of 1 h. Each cycle consisted of one heating and one cooling process. Based on the number of cycles, the granite specimens were divided into different groups: 0 cycles (untreated), and 3, 5, 7, 9, 15, and 20 cycles. Multiple parallel samples were prepared for each group to ensure validity and reliability.

In order to assess the damage caused by high-temperature heating and liquid nitro-gen cooling on the granite, ultrasonic testing was performed both before and after the pretreatment of the specimens. This allowed for the evaluation of any changes in the internal structure and integrity of the rock. After the pretreatment of the granite was completed, three-point bending tests and cross-sectional scanning experiments were conducted. These tests measured the mechanical properties and examined the microstructural changes of the granite specimens.

## **3. Investigation of the Mechanical Behavior of Granite**

### *3.1. Experimental Results of Mechanical Properties*

The load displacement curves of granite under different heating and liquid nitrogen cooling cycles are shown in Figure 3. Initially, during the densification stage, the overall slope of the granite sample's curve decreased, indicating the development of internal cracks induced by high-temperature heating. These cracks, along with the presence of thermal stresses, contributed to this observation. Subsequently, as the granite sample underwent liquid nitrogen cooling, cold shrinkage of the particles further promoted crack propagation. With repeated thermal loading and cooling cycles, the cracks became extensive and interconnected, resulting in significant displacements even under relatively small loads. Moreover, an increase in the number of cycles led to a hardening effect due to the thermal treatment. Although this effect did not impact the development of internal cracks, it enhanced the sample's resistance to failure during the initial densification stage.

In the elastic stage, the load–displacement curve demonstrated minimal variations but generally displayed a decreasing trend with an increasing number of cycles. Additionally, the duration of the elastic stage gradually reduced as more cycles were performed, which can be attributed to the progressive development of cracks within the granite sample. This crack propagation ultimately weakened the overall strength of the sample. During the crack propagation stage, as the external load continued to increase, the cracks within the granite sample developed further, accompanied by the generation of numerous microcracks. Failure occurred when the peak load that the granite sample could withstand was reached. At this stage, both the peak load and the displacement experienced by the granite sample decreased with an increasing number of cycles. The cyclic loading process induced deformation and damage in the granite, degrading its mechanical properties. While granite initially exhibited ductile behavior and withstood substantial loads, fatigue damage accumulated within its internal microstructure with an increasing number of cycles, resulting in diminished strength and stiffness. Consequently, the rock's capacity to endure peak loads was reduced, and the displacement of the granite sample gradually diminished as well. This phenomenon can be attributed to the impact of damage and plastic deformation on the rock's deformation capacity. Moreover, a higher number of thermal loading and cooling cycles caused the granite sample's failure-resistance to reach its limit and subsequently decline, leading to a sharp decrease in the load it was able to withstand at the point of failure, along with a rapid reduction in displacement.

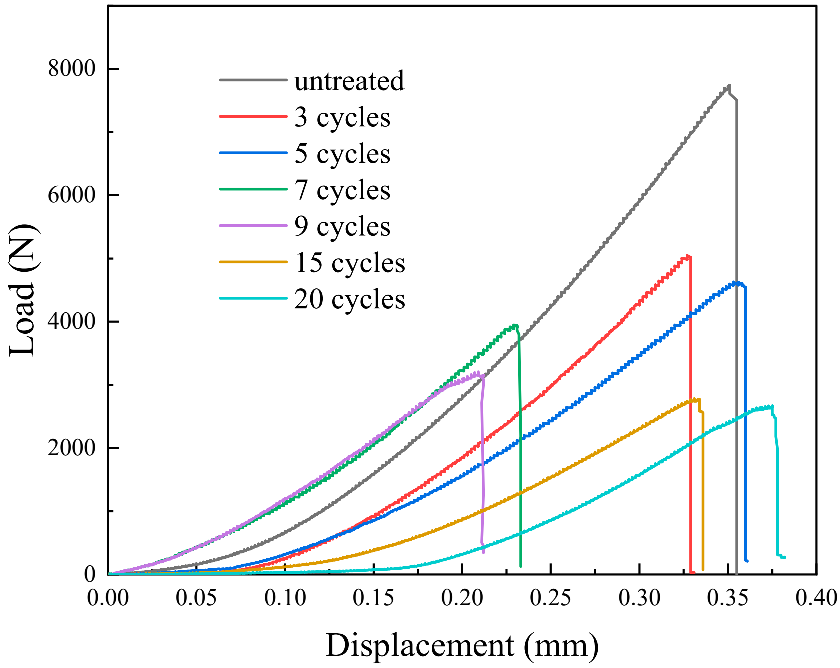


**Figure 3.** Load–displacement curve.

### *3.2. Analysis of Acoustic Emission Characteristics of Granite*

Under the influence of external factors, such as external forces and temperature, materials may experience deformation and failure due to stress fluctuations at defective sites, which can impact their structural integrity. This process leads to the rapid release of localized energy, generating transient elastic waves known as acoustic emission (AE) [38]. Valuable insights into the damage characteristics during rock loading can be obtained through the conduction of acoustic emission (AE) experiments, collection of AE signals from rocks, and meticulous processing and analysis. In order to assess the extent of rock damage, we analyze the variations in characteristic parameters. The variation of the ringing count during the deformation and failure process of granite under different heating and liquid nitrogen cooling cycles is shown in Figure 4.

Based on the analysis of Figure 4, a close correlation between the failure stages of the granite specimen in the three-point bending test and the variations in acoustic emission ring-down count becomes evident. In the initial compaction stage, the applied load on the specimen remains relatively modest, leading to a low rate of acoustic emission ring-down count and the presence of stable signals. Furthermore, the curve depicting the cumulative ring-down count indicates minimal growth with a consistent pattern. During this stage, the acoustic emission signals primarily arise from the relative sliding and friction between particles within the rock. In the subsequent elastic phase, the acoustic emission ring-down signals exhibit limited activity compared to the compaction phase. However, this stage manifests enhanced magnitudes of events and a progressive increase in the cumulative ringing count, characterized by an ascending slope in the plot. This phenomenon arises due to the prevalence of microcracks and subtle self-adjustments occurring within the granite, aiming to optimize its load-carrying capacities.

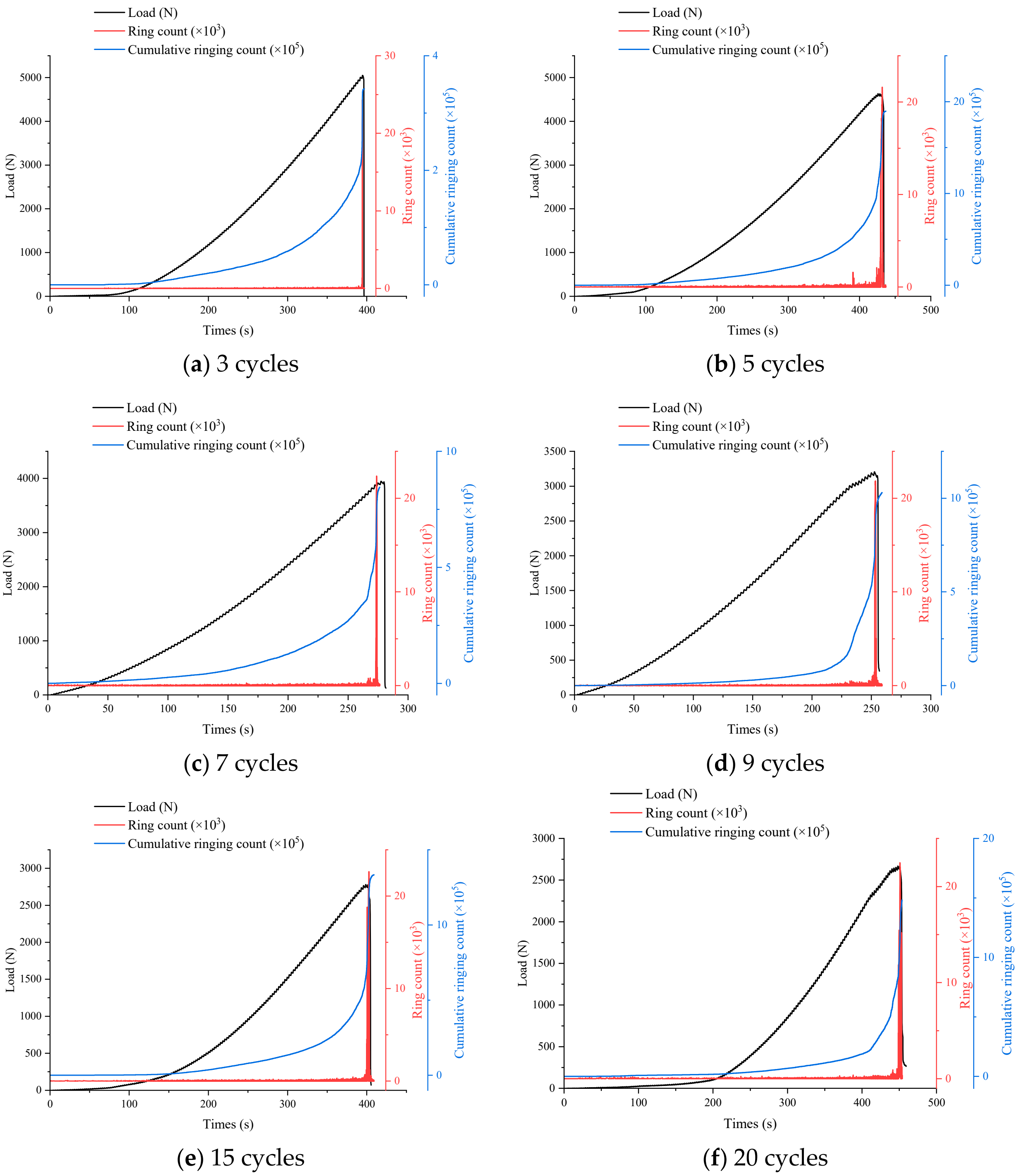


(**a**) 3 cycles (**b**) 5 cycles

(**c**) 7 cycles (**d**) 9 cycles

(**e**) 15 cycles (**f**) 20 cycles

**Figure 4.** Variation patterns of ringing count in granite.

Under specific cyclic conditions, certain specimens display thousands of ringing counts, accompanied by abrupt shifts in the cumulative ringing count. These observations can be attributed to recurrent thermal treatments that undermine the gentle nature of the granite and its resistance to deformation induced failure. Upon reaching the yield phase, a significant surge in the acoustic emission ringing count occurs, indicating intensified signal activity and the emergence of multiple pronounced peaks. Concurrently, the cumulative ringing count experiences a rapid upsurge, accompanied by notable fluctuations in magnitude and a steep ascent in the curve's gradient. At this stage, the rock triggers fracturing mechanisms, resulting in the proliferation of microcracks that amalgamate to form interconnected macroscopic fissures. In the failure phase, there is a precipitous escalation in the acoustic emission ring-down count. At the instant when the applied load attains its pinnacle, which represents the maximum capacity the specimen can endure, the ring-down count also reaches its zenith, simultaneously with a pronounced augmentation in the cumulative ring-down count. Subsequently, as the specimen undergoes complete structural failure rendering it incapable of bearing any load, the dissipation of stress in the rock mass rapidly dwindles until it dissipates altogether.

Figure 5 illustrates the relationship between the cumulative ring count and the number of cycles performed, displaying an initial decrease before a subsequent increase. This trend is indicative of a cyclic process involving damage and repair within the rock during loading. Upon exposure to external loading, internal stress concentration intensifies, and as the loading cycles accumulate over time, microcracks within the rock gradually extend, resulting in heightened acoustic emission events and an elevation in the ring-down count. However, it is crucial to acknowledge that the loading process also triggers elastic reconstitution and crack closure within the rock, leading to a reduction in the ring-down count. These cyclical variations contribute to the observed trend of an initial decrease followed by an increase in the cumulative ring-down count. Furthermore, other factors influencing fluctuations in the ring-down count include variations in crack structures, nonhomogeneous stress distribution, and the inherent physical properties of the rock. The observed initial decrease followed by a subsequent increase in the cumulative ring-down count can be attributed to the dynamic interplay between damage and recovery processes taking place within the rock during the loading process.

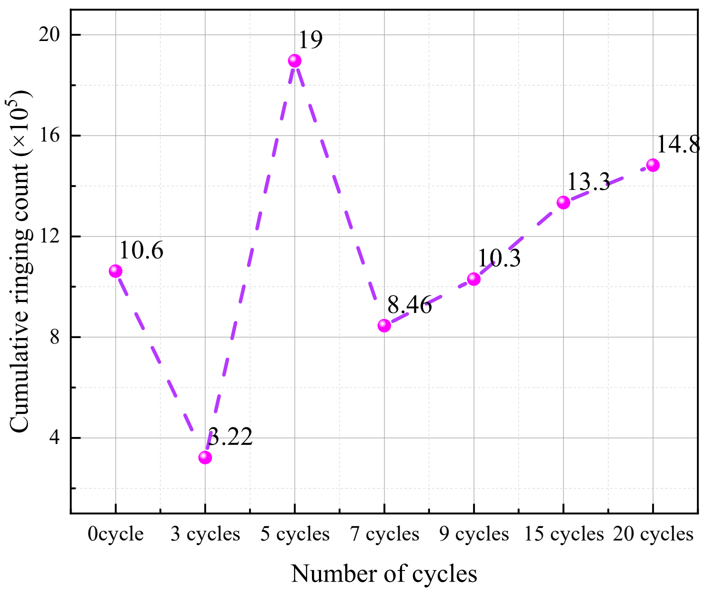


**Figure 5.** Relationship between cumulative ringing count and number of cycles.

According to Figure 6, the energy counts in the deformation and destruction process of granite under different heating and liquid nitrogen cooling conditions exhibit a similar pattern to the ring counts. In the initial loading stage, when the applied load on the granite is relatively small, the energy counts remain low. As the load increases, the energy counts significantly rise, and as it approaches the peak load of the granite, the cumulative energy counts show an exponential growth trend. Moreover, as the number of cycles of high-temperature heating and liquid nitrogen cooling increases, the compaction stage of the granite expands, and the cumulative energy counts curve nearly levels off (Figure 6e,f).

This is because multiple cycles of liquid nitrogen treatment cause damage to the interior of the rock, resulting in the formation of more microcracks. With consecutive cyclic treatments, the connections between particles inside the granite become disrupted, making the rock more susceptible to fracture and generating more acoustic emission signals. The research findings suggest that high-temperature heating and liquid nitrogen cooling can intensify internal structural damage in the rock, leading to the formation of additional pores and microcracks in granite. With an increase in external load, the interconnected microcracks facilitate the development of a complex network of fractures. This phenome-non highlights the significant potential of liquid nitrogen fracturing technology in trans-forming high-temperature reservoir rocks.

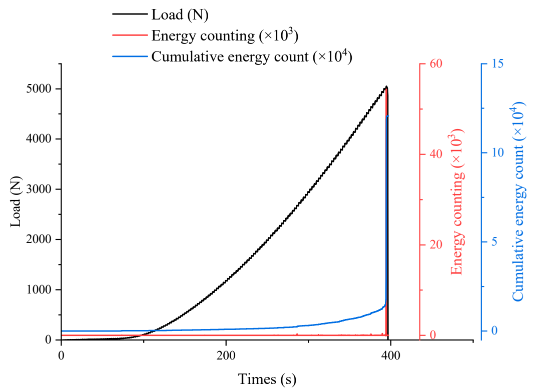


(**a**) 3 cycles

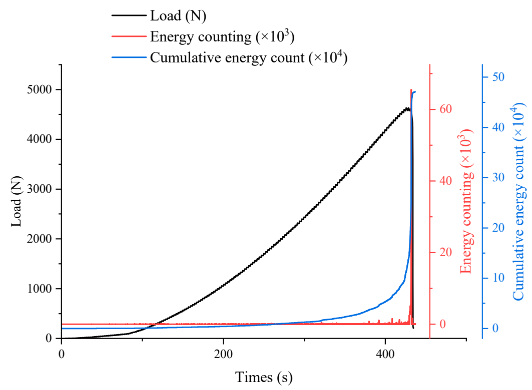


(**b**) 5 cycles

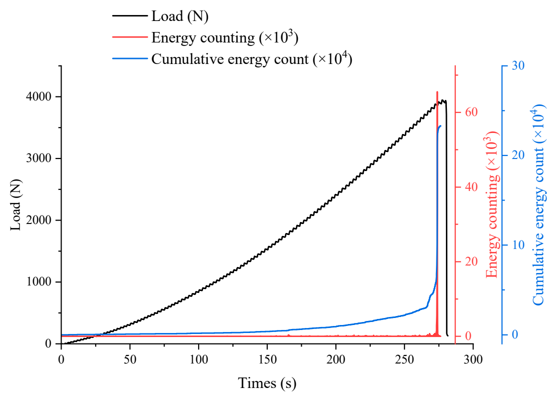


(**c**) 7 cycles

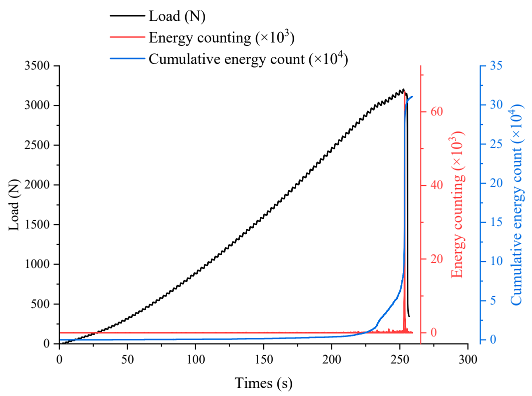


(**d**) 9 cycles

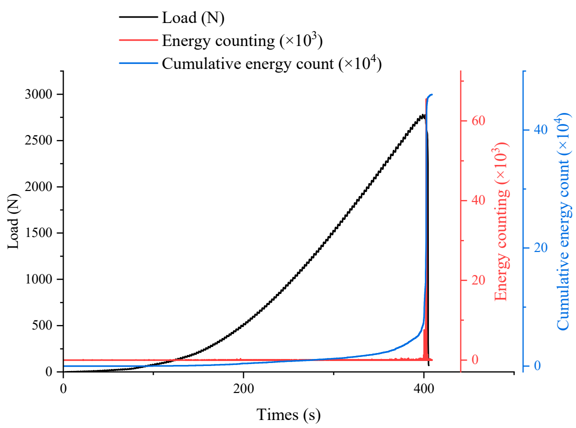


(**e**) 15 cycles

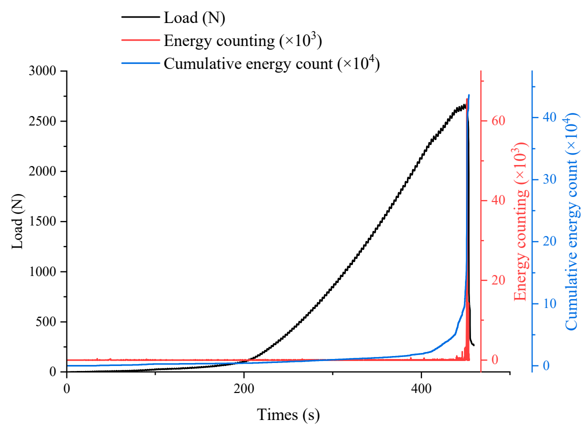


(**f**) 20 cycles

**Figure 6.** Variation patterns of energy count in granite.

### 3.3. Energy Analysis of Granite

The trend of the energy absorbed by granite under different heating and liquid nitrogen cooling cycles with load variation is shown in Figure 7, which helps us further explore the energy evolution characteristics of granite. It can be observed that prior to the failure of the granite, the energy absorbed by granite increases with the increase in load, and the energy is proportional to the load. This is because the energy applied to the granite before it fractures is stored inside the rock as elastic energy. In addition, upon comparing the energy trends of granite under different liquid nitrogen cooling cycles, it can be observed that the larger the number of cycles, the smaller the total energy absorbed by the granite. This implies that the load-bearing capacity of granite decreases considerably with multiple heating and liquid nitrogen cooling cycles. The same conclusion can also be derived from the load displacement curve of granite.

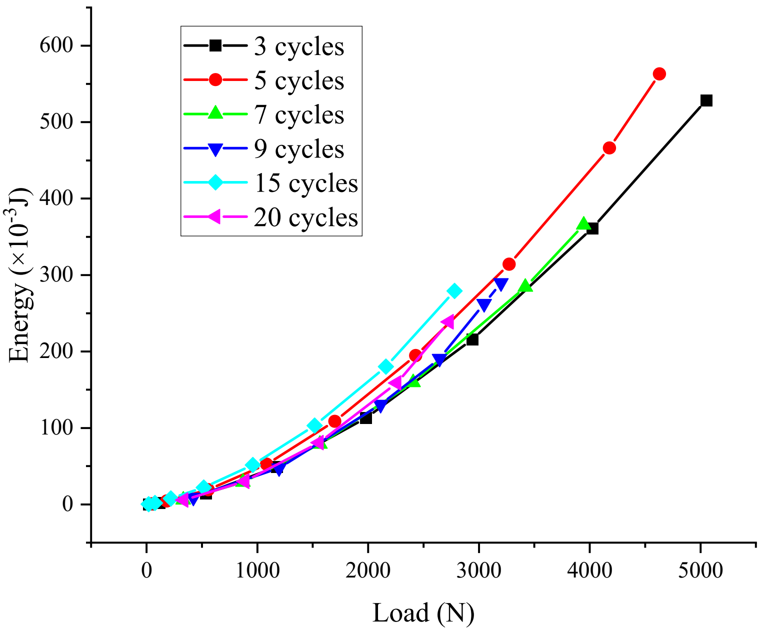


**Figure 7.** Cycle group load−energy diagram.

Overall, these observations indicate that heating and liquid nitrogen cooling cycles can lead to a reduction in the load-bearing capacity of granite and may cause significant damage to the internal structure of the rock. As such, understanding the energy evolution characteristics of granite under different heating and cooling conditions is vital for predicting the behavior of rocks under external loads and optimizing the design of reservoir stimulation technologies.

The fitting diagram of granite peak energy and load is shown in Figure 8. Upon fitting the peak energy and load, it is apparent that there exists a close relationship between the two variables. However, instead of demonstrating linearity, the fitting curve exhibits nonlinearity. This is primarily because granite is not a fully elastic material, and therefore, energy cannot be entirely converted into elastic energy and stored within the rock. Furthermore, after undergoing multiple high-temperature heating and liquid nitrogen cooling cycles, numerous microcracks or damage occur within the granite. The presence of these microcracks results in energy dissipation and weakens the strength and load-bearing capacity of the granite. Consequently, as the number of cycles increases, the energy that can be stored within the granite gradually decreases, rendering the rock more susceptible to failure.

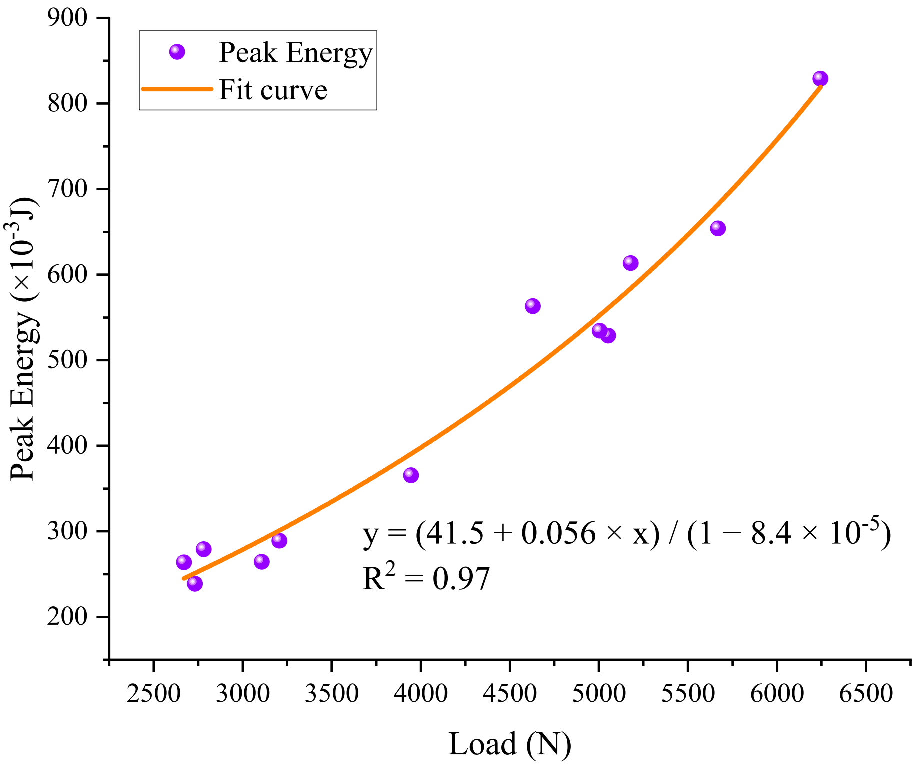


**Figure 8.** Relationship between peak load and total energy of cycle group and its fitting results.

It is important to recognize that this nonlinearity in the relationship between peak energy and load in granite arises from the inherent characteristics of the rock itself, including its nonelastic behavior and the generation of microcracks during cyclic treatments. Understanding such relationships and the associated energy evolution is crucial for accurately assessing the performance and reliability of granite under various loading conditions, especially in the context of repeated heating and liquid nitrogen cooling cycles.

## 4. Microstructural Changes in Granite

### *4.1. Granite Wave Velocity Analysis*

Ultrasound plays a significant role in practical engineering applications for rock mechanics, particularly in detecting crack development and structural changes within rock masses. The propagation speed of ultrasonic waves is primarily influenced by factors such as the composition of the propagation medium within the rock mass and its porosity. Different media exhibit varying propagation speeds of ultrasonic waves. When passing through rocks, the presence of cracks can cause scattering or waveform changes in the ultrasonic waves [39].

The relationship between the velocity of longitudinal waves in rocks and the number of cycles is shown in Figure 9. This figure illustrates the impact of the number of cycles on the internal longitudinal wave velocity of rocks. It is evident that as the number of cycles increases, the P-wave velocity of granite experiences a notable decrease. This indicates that high-temperature heating and liquid nitrogen cooling have induced damage within the rock, altering the propagation speed of ultrasound. It is worth noting that between 15 and 20 cycles, the magnitude of wave velocity variation in granite is not substantial, suggesting that the growth of damage within granite does not increase indefinitely with an increasing number of cycles. Therefore, during the actual engineering application of liquid nitrogen fracturing, it is crucial to select a more reasonable treatment frequency to achieve maximum benefits.

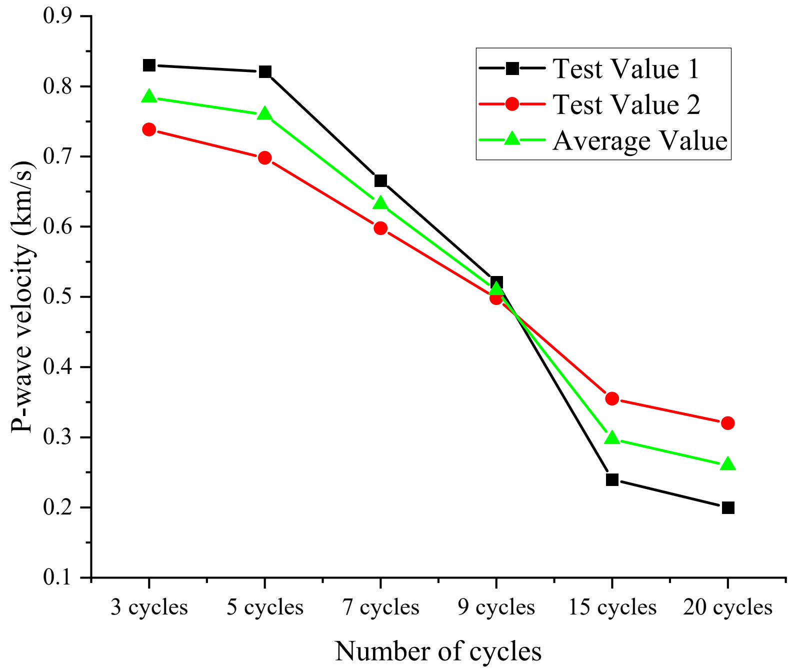


**Figure 9.** P-wave velocity of granite under different cycles.

*4.2. Scanning Section Analysis of Granite*

The granite specimens were subjected to a controlled process involving precise high-temperature heating, followed by rapid cooling through the application of liquid nitrogen. Subsequently, incremental external loading was applied to the specimens. When the critical load limit that the granite could sustain was reached, inevitable fracturing phenomena were observed, manifesting as macroscopically visible fissures. However, it is important to note that in addition to these visible fissures, the granite matrix may also contain imperceptible microscale cracks. To comprehensively investigate the influence of varying cycle numbers on the extent of failure in the granitic specimens, a cutting-edge three-dimensional scanning system, specifically the VR-5000 series 3D profilometer, was employed. This state-of-the-art technology facilitated meticulous profiling and morphological analysis of the treated granite samples. By utilizing the capabilities of this system, we were able to capture detailed surface morphology and gain insights into the presence and characteristics of cracks, fissures, and other structural changes at a micro-scale level.

The fracture surfaces of granite specimens that underwent multiple cycles were scanned using the VR-5000 series 3D profilometer, and the obtained data were subjected to calculations. Employing fractal theory, the fractal dimension of the fracture surface was quantitatively determined to assess the micro fracture characteristics of the granite. The characteristics of the granite fracture surfaces under different cycles and their respective fractal dimensions are shown in Figure 10. Observations indicate a notable increase in surface roughness as the number of cycles increases. Clear elevations in valley depth and peak height are discernible, while the fault surface exhibits significant fluctuations. This behavior can be attributed to the synergistic effects of high-temperature exposure and liquid nitrogen cooling. These processes promote the interconnection between pre-existing microcracks within the granite and those induced by the application of liquid nitrogen, resulting in the formation of weakened areas. Consequently, the overall mechanical properties of the rock are compromised. As external loads intensify, the weak areas experience initial rupture, facilitating the formation of extensive and intricate fracture networks within the rock mass. This phenomenon enhances the vulnerability of the granite and contributes to the development of large-scale fractures with complex geometries.

The fractal dimensions and the trends of maximum and minimum heights of granite fracture surfaces after various cyclic treatments are shown in Figures 11 and 12. These parameters serve to further assess the roughness and complexity of the fracture surfaces. Upon analysis of the fractal dimension and fracture surface height, it is evident that the cyclic treatment involving high-temperature heating and liquid nitrogen cooling results in an upward trend for both parameters. This signifies an enhancement in the roughness and complexity of the cross-sectional features. The underlying cause of this phenomenon lies in the alternating effects of high-temperature heating and liquid nitrogen cooling. As the internal particles within the granite undergo continuous expansion and contraction due to the cyclic treatment, the development of microcracks is promoted. Subsequently, the application of external loads triggers further propagation of these internal cracks, greatly augmenting the complexity of the fracture surface morphology. In practical engineering applications, these intricate cross-sectional features contribute to the expansion of the contact area between heat exchange substances and reservoir rocks. This holds significant implications for the improvement of geothermal energy development efficiency.

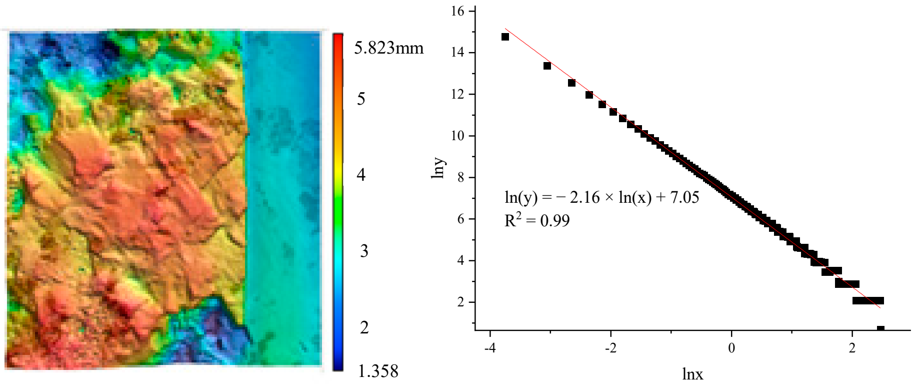


(**a**) 3 cycles

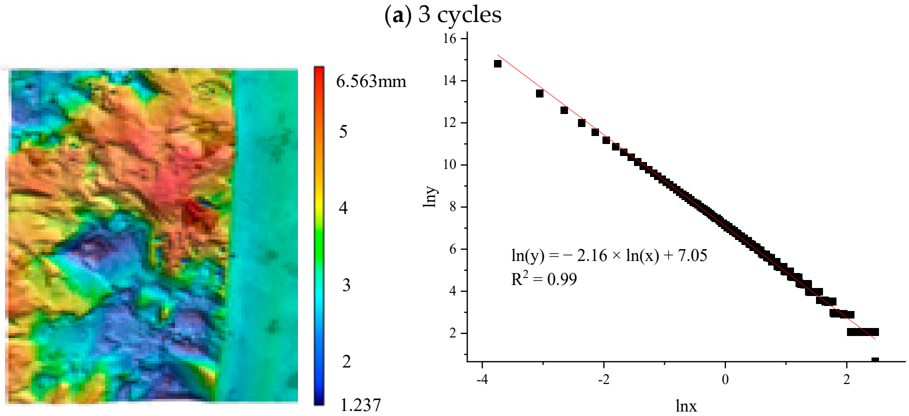


(**b**) 5 cycles

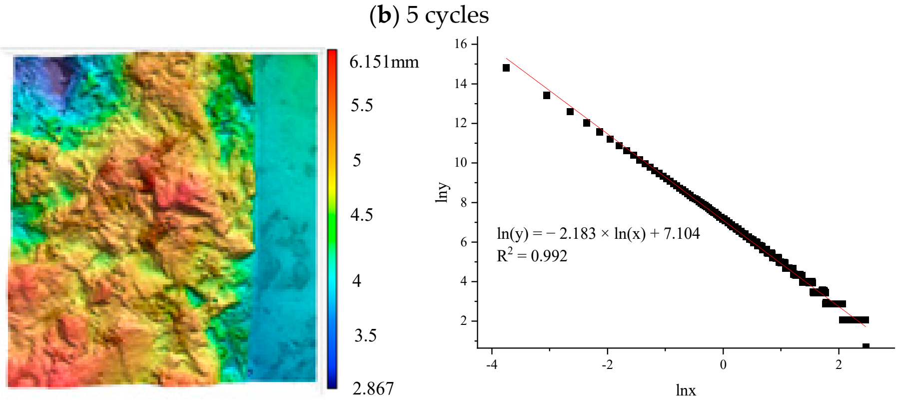


(**c**) 7 cycles

**Figure 10.** *Cont.*

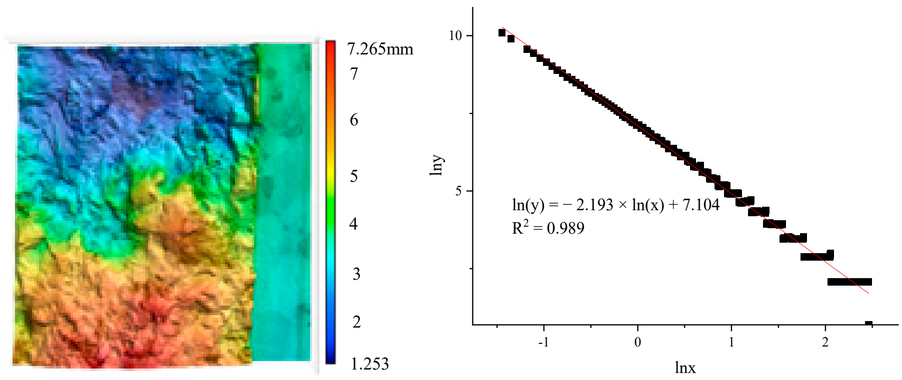


(**d**) 9 cycles

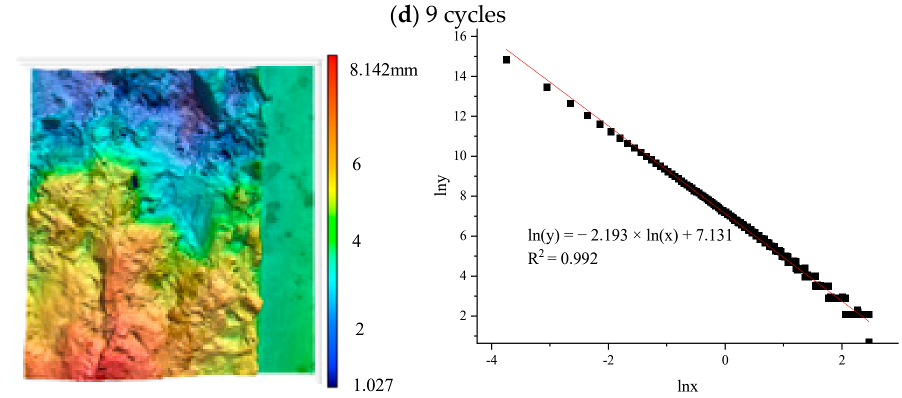


(**e**) 15 cycles

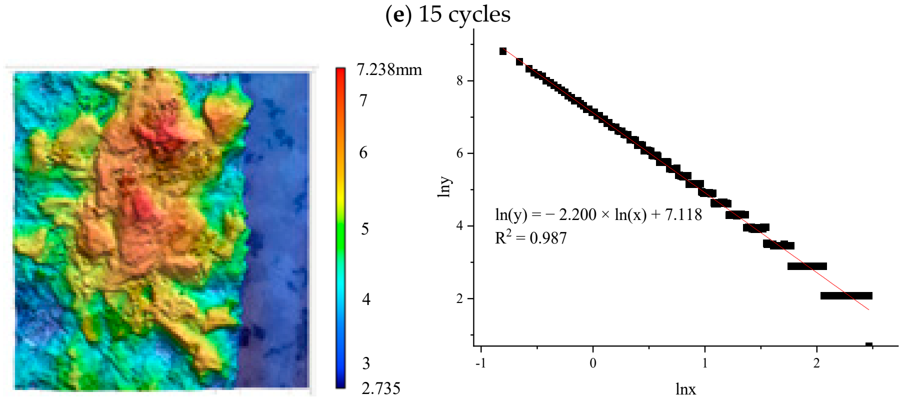


(**f**) 20 cycles

**Figure 10.** The features of granite fracture surfaces under varying cycle numbers.

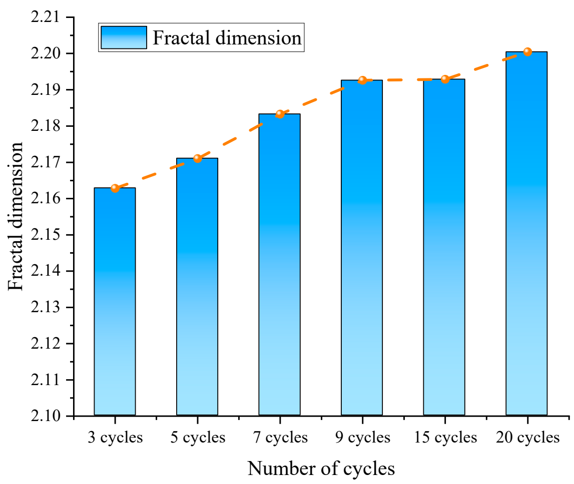


**Figure 11.** Fractal dimension of granite sample section under different cycles.

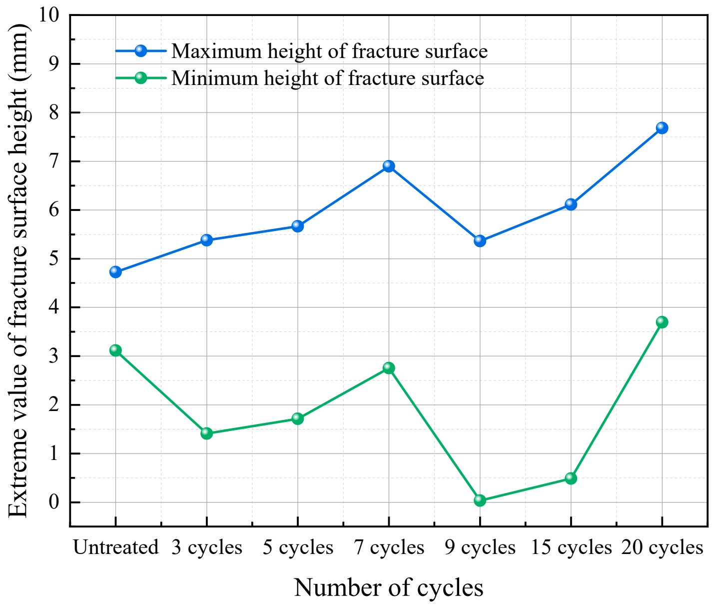


**Figure 12.** Maximum and minimum heights of granite sample sections under different cycles.

*4.3. Analysis of High-Temperature Fracture Toughness in Granite*

Fracture toughness is a crucial property that characterizes the ability of rocks to resist the propagation of internal cracks. The analysis of the surface morphology of fractured rocks typically reveals three primary modes: opening, sliding, and tearing. Tearing mode predominates in the fracture surfaces of rocks. Fracture toughness of rocks can be evaluated using a three-point bending test, and the relevant calculations can be performed using Equations (1)–(4) [23,25].

$$S' = \frac{S}{2R} \tag{1}$$

$$a' = \frac{a}{R} \tag{2}$$

$$Y = -1.297 + 9.516S' - (0.47 + 16.457S')a' + (1.071 + 34.401S')a'^2 \tag{3}$$

$$K_{IC} = \frac{P_{\max}\sqrt{\pi a}}{2RB}Y \tag{4}$$

Among these parameters, $S$ represents the distance between support points, and $a$ denotes the crack depth, with a specific value of 14 mm. $R$ signifies the radius, measured at 38 mm, while $B$ corresponds to the width, defined as 30 mm. $K_{IC}$ stands for fracture toughness, and $Y$ represents the associated factor.

Based on the ISRM guidelines for type I quasistatic fracture toughness testing of rock-like materials, the distance between support points $(S)$ and twice the sample diameter $(2R)$ should satisfy the condition $0.5 \leq S' \leq 0.8$. Thus, in this experiment, the ratio is chosen as 0.5, resulting in $S$ = 38 mm [40].

Based on the provided values, substituting them into Equations (1) and (2) yields the values of $S' = 0.5$ and $a' = 0.368$. Subsequently, substituting these results into Equation (3) allows for the determination of $Y = 2.734$.

The fracture toughness of each specimen under various conditions can be determined by combining the aforementioned values with the maximum load values obtained during different cycles, as shown in Figure 13.

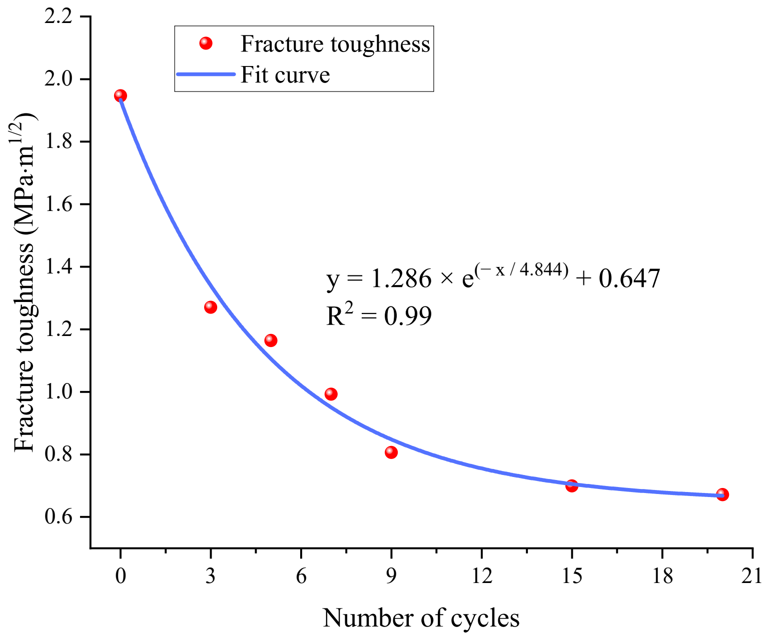


**Figure 13.** Change of fracture toughness of granite samples under different cycles.

The changes in fracture toughness of granite during multiple cycles are shown in Figure 13. Evidently, an escalation in high-temperature heating and liquid nitrogen cooling cycles instigates a rapid decline in the fracture toughness of granite. As liquid nitrogen cools the heated rocks, it induces instantaneous thermal stress that prompts surface cracking under colder conditions. The vast temperature differential between the high-temperature granite and the low-temperature liquid nitrogen engenders internal thermal stress within the rock, subsequently resulting in thermally-induced fractures. With each successive cycle, microcracks proliferate and intersect, amplifying the extent of the damage and rendering the granite increasingly susceptible to tensile failure. The research findings reliably indicate the profound capability of liquid nitrogen cooling to significantly impair the mechanical properties of rocks, thereby giving rise to a heightened prevalence of microcracks within their structures. Under applied loads, these microcracks rapidly propagate, ultimately forming intricate three-dimensional networks of fractures. Consequently, the utilization of liquid nitrogen as a viable approach for augmenting permeability in dry hot rock reservoirs holds considerable promise.

In addition, when actual liquid nitrogen is injected into high-temperature reservoir rocks, liquid nitrogen as a fluid will undergo fluid flow and heat transfer in the reservoir rocks. We assume that rock is an ideal thermoelastic body that may cause certain thermal expansion or contraction, resulting in deformation and stress. We believe that the contribution of seepage and heat transfer to stress is [41]:

$$\sigma_{ij} = 2G\varepsilon_{ij} + \frac{2G\nu}{1-2\nu}\delta_{ij}\varepsilon_{kk} - K\alpha_T\delta_{ij}T - \alpha\delta_{ij}p \tag{5}$$

the mechanical equilibrium equation including the coupling term can be obtained in terms of displacement [42]:

$$G\mu_{i,jj} + \frac{G}{1-2\nu}\mu_{j,ji} - K\alpha_T T_{,i} - \alpha p_{,i} + F_i = 0 \tag{6}$$

The heat transfer process between liquid nitrogen and high-temperature granite involves heat conduction and convection. We can use the heat conduction equation to describe the heat conduction process between liquid nitrogen and rocks. This equation considers the thermal diffusion properties of liquid nitrogen and rocks, as well as the temperature gradient between them, thus describing the transfer process of thermal energy. Assuming that solids and fluids are always in a local thermal equilibrium state:

$$(\rho C)_{eff}\frac{\partial T}{\partial t} + KT\alpha_T\frac{\partial \varepsilon_v}{\partial t} + \rho_l C_l T\frac{k}{\mu}\nabla p\nabla T - \lambda_{eff}\nabla^2 T = Q_T \tag{7}$$

It should be pointed out that due to the significant temperature difference between liquid nitrogen and high-temperature granite, as well as the involvement of phase transitions and complex interactions, this issue may be more complex. In practical applications, it may be necessary to combine numerical simulation and experimental verification, and further refine and adjust the mathematical model based on specific material properties and situations to obtain more accurate results.

To summarize, previous studies on liquid nitrogen-induced rock fracturing have primarily focused on the macroscopic mechanical properties of rocks, while the underlying mechanisms remain unclear. This study specifically investigates the characteristics of mode I fractures in granite under the influence of liquid nitrogen cooling. It examines the impact of cold temperature on high-temperature rocks, analyzes acoustic emission characteristics, and examines microscopic crack propagation using methods such as three-point bending tests and ultrasonic detection. The study also suggests the need for further research on the optimal number of liquid nitrogen treatments. Overall, the findings shed light on the evolutionary behavior of cracks in granite subjected to high-temperature heating and liquid nitrogen cooling, providing valuable insights into rock fracture behavior and its implications for enhancing geothermal reservoir production.

## 5. Conclusions

In this study, we investigated the evolutionary characteristics of mode I fractures in granite under continuous high-temperature heating and liquid nitrogen cooling treatment. To comprehensively understand the behavior of microcracks within rocks after liquid nitrogen cooling and the roughness characteristics of micro-cross-sections, we employed several testing techniques, including ultrasonic testing, acoustic emission testing, and cross-sectional scanning analysis. The experimental findings offer detailed insights into the propagation modes and development characteristics of internal microcracks, as well as the roughness characteristics of micro cross-sections. The specific research results are summarized as follows:

(1) High-temperature heating and liquid nitrogen cooling cycling treatment significantly diminish the mechanical properties of granite. With an increasing number of cycles, the I-mode fracture toughness of granite gradually decreases. However, beyond a certain threshold, the degree of damage to the granite no longer exhibits a significant increase.

(2) The cyclic heating and liquid nitrogen cooling treatment improve the ductility characteristics of granite. The substantial thermal stress induces the propagation and proliferation of microcracks within the rock, prolonging the compaction stage of the granite. As the number of cycles increases, the ultimate bearing capacity of granite decreases significantly, while the elastic energy stored inside the rock decreases, resulting in improved ductility.

(3) Fractal dimension and fracture surface characteristic parameters were used for quantitative evaluation of rock fracture surfaces. It was found that a higher number of cycles leads to the formation of more complex fracture surfaces. Multiple thermal and cold shocks weaken the bonding between rock mineral particles, making it easier for cracks to develop within the rock. Under loading, microcracks propagate and intersect, forming a complex network of cracks.

(4) The significant temperature difference between high-temperature granite and low-temperature liquid nitrogen is the primary reason for the decrease in rock mechanical properties. Cyclic heating and liquid nitrogen cooling treatment can induce fatigue dam-age, further reducing the rock's bearing capacity and making it more prone to

fracturing. The initiation, development, and propagation of microcracks within rocks contribute to the formation of large-scale fractures with complex geometric shapes in geothermal reservoirs, providing seepage channels and promoting geothermal reservoir production.

Overall, this study reveals the evolutionary characteristics of crack behavior in granite subjected to high-temperature heating and liquid nitrogen cooling treatment, which holds great significance in understanding the fracture behavior of rocks and their implications for geothermal reservoir stimulation.

## Nomenclatures

| | |
|---|---|
| $a$ | Crack depth of the semi-circular bend specimen |
| $B$ | Width of the semi-circular bend specimen |
| $G$ | Shear modulus |
| $h$ | Convective heat transfer coefficient |
| $K$ | Drainage bulk modulus |
| $K_{IC}$ | Fracture toughness |
| $p$ | Pore water pressure |
| $P_{\max}$ | Peak load |
| $Q_T$ | Convective heat flux |
| $R$ | Radius of the semi-circular bend specimen |
| $S$ | Distance between support points |
| $T_{ext}$ | Temperature of the injected fluid |
| $\mu_i$, $\mu_j$ | Displacement component |
| $\nu$ | Poisson's ratio |
| $Y$ | Associated factor |
| $\alpha_T$ | Thermal expansion coefficient of the rock |
| $\alpha$ | Biot's coefficient |
| $\sigma_{ij}$ | Stress component |
| $\varepsilon_{ij}$ | Strain component |
| $\delta_{ij}$ | Kronecker number |

**Author Contributions:** Conceptualization, L.W.; Methodology, Y.X. and Z.C.; Data curation, H.K., J.H. and Z.Z. All authors have read and agreed to the published version of the manuscript.

**Funding:** This research was funded by National Natural Science Foundation of China (52004082, 52274096, 12202353 and 12002270.

**Data Availability Statement:** The data used to support the findings of this study are included within the article.

**Conflicts of Interest:** The authors declare that they have no conflict of interest.

## References

1. Jiang, L.; Cui, Y.; Wang, H.; Sun, F.; Wang, X.; Du, J. Spatiotemporally Chemical Variations of Groundwater in the Southeastern of Liaoning Province. *Earthquake* **2021**, *41*, 114–130.
2. Liu, J.; Xue, Y.; Fu, Y.; Yao, K.; Liu, J. Numerical investigation on microwave-thermal recovery of shale gas based on a fully coupled electromagnetic, heat transfer, and multiphase flow model. *Energy* **2023**, *263*, 126090. [CrossRef]
3. Khan, N.S.; Sriyab, S.; Kaewkhao, A.; Thawinan, E. Hall current effect in bioconvection Oldroyd-B nanofluid flow through a porous medium with Cattaneo-Christov heat and mass flux theory. *Sci. Rep.* **2022**, *12*, 19821. [CrossRef] [PubMed]
4. Deng, L.; Li, X.; Wu, Y.; Li, F.; Huang, Z.; Ji, Y.; Zou, C.; Liu, Z. Influence of cooling speed on the physical and mechanical properties of granite in geothermal-related engineering. *Deep Undergr. Sci. Eng.* **2022**, *1*, 40–57. [CrossRef]
5. Wang, J.; Wang, H.; Wang, X.; Yang, S.; Wu, H.; Leung, C.; Tian, J. A multiphysical-geochemical coupling model for caprock sealing efficiency in $CO_2$ geosequestration. *Deep Undergr. Sci. Eng.* **2023**, *2*, 188–203. [CrossRef]
6. Khan, N.S.; Hussanan, A.; Kumam, W.; Kumam, P.; Suttiarporn, P. Accessing the thermodynamics of Walter-B fluid with magnetic dipole effect past a curved stretching surface. *ZAMM-J. Appl. Math. Mech./Z. Angew. Math. Und Mech.* **2023**, *103*, e202100112. [CrossRef]
7. Soltani, M.; Kashkooli, F.M.; Souri, M.; Rafiei, B.; Jabarifar, M.; Gharali, K.; Nathwani, J.S. Environmental, economic, and social impacts of geothermal energy systems. *Renew. Sustain. Energy Rev.* **2021**, *140*, 110750. [CrossRef]

8. Zhao, Y.; Yang, D.; Feng, Z.; Liang, W.; Kang, Z. Multi-field coupling theory of porous media and its applications to resources and energy engineering. *Chin. J. Rock Mech. Eng.* **2008**, *27*, 1321–1328.
9. Wang, S.; Zhang, W.; Zhang, G.; Sun, Z. Exploitation and development trend of unconventional energy. *China Min. Mag.* **2013**, *22*, 5–8.
10. Ali, J.A.; Hamadamin, A.B.; Ahmed, S.M.; Mahmood, B.S.; Sajadi, S.M.; Manshad, A.K. Synergistic effect of Nanoinhibitive drilling fluid on the shale swelling performance at high temperature and high pressure. *Energy Fuels* **2022**, *36*, 1996–2006. [CrossRef]
11. Guo, P.; Wu, B.; Li, P.; Liu, W. Research progress on hydrofracture and evaluation of enhanced geothermal system. *Resour. Environ. Eng.* **2020**, *34*, 256.
12. Wu, X.; Huang, Z.; Song, H.; Zhang, S.; Cheng, Z.; Li, R.; Wen, H.; Huang, P.; Dai, X. Variations of physical and mechanical properties of heated granite after rapid cooling with liquid nitrogen. *Rock Mech. Rock Eng.* **2019**, *52*, 2123–2139. [CrossRef]
13. Wang, X.; Wu, N.; Su, Z.; Zeng, Y. Progress of the enhanced geothermal systems (EGS) development technology. *Prog. Geophys.* **2012**, *27*, 355–362.
14. King, S.R. Liquid $CO_2$ for the stimulation of low-permeability reservoirs. In Proceedings of the SPE/DOE Low Permeability Gas Reservoirs Symposium, Denver, CO, USA, 14–16 March 1983.
15. Mcdaniel, B.W.; Grundmann, S.R.; Kendrick, W.D.; Wilson, D.R.; Jordan, S.W. Field applications of cryogeni-c nitrogen as a hydraulic fracturing fluid. In Proceedings of the SPE Annual Technical Conference and Exhibition, San Antonio, TX, USA, 5–8 October 1997.
16. Grundmann, S.R.; Rodvelt, G.D.; Dials, G.A.; Allen, R.E. Cryogenic Nitrogen as a Hydraulic Fracturing Fluid in the Devonian Shale. In Proceedings of the SPE Eastern Regional Meeting, Pittsburgh, PA, USA, 9–11 November 1998.
17. Cha, M.; Yin, X.; Kneafsey, T.; Johanson, B.; Alqahtani, N.; Miskimins, J.; Patterson, J.; Wu, Y. Cryogenic fracturing for reservoir stimulation–Laboratory studies. *J. Pet. Sci. Eng.* **2014**, *124*, 436–450. [CrossRef]
18. Cai, C.; Li, G.; Huang, Z.; Shen, Z.; Tian, S. Rock pore structure damage due to freeze during liquid nitrogen fracturing. *Arab. J. Sci. Eng.* **2014**, *39*, 9249–9257. [CrossRef]
19. Gao, Q.; Cheng, Y.; Han, S.; Yan, C.; Li, Y.; Han, Z. Effect of shale matrix heterogeneity on gas transport during production: A microscopic investigation. *J. Pet. Sci. Eng.* **2021**, *201*, 108526. [CrossRef]
20. Zhang, S.; Huang, Z.; Li, G.; Wu, X.; Peng, C.; Zhang, W. Numerical analysis of transient conjugate heat transfer and thermal stress distribution in geothermal drilling with high-pressure liquid nitrogen jet. *Appl. Therm. Eng.* **2018**, *129*, 1348–1357. [CrossRef]
21. Zhang, S.; Huang, Z.; Wang, H.; Li, G.; Sepehrnoori, K.; Wu, X.; Hong, C. Experimental study on the rock-breaking characteristics of abrasive liquid nitrogen jet for hot dry rock. *J. Pet. Sci. Eng.* **2019**, *181*, 106166. [CrossRef]
22. Yang, R.; Huang, Z.; Shi, Y.; Yang, Z.; Huang, P. Laboratory investigation on cryogenic fracturing of hot dry rock under triaxial-confining stresses. *Geothermics* **2019**, *79*, 46–60. [CrossRef]
23. Yin, T.; Li, Q.; Li, X. Experimental investigation on mode I fracture characteristics of granite after cyclic heating and cooling treatments. *Eng. Fract. Mech.* **2019**, *222*, 106740. [CrossRef]
24. Wang, L.; Xue, Y.; Cao, Z.; Wu, X.J.; Dang, F.N.; Liu, R. Mechanical Properties of High-Temperature Granite under Liquid Nitrogen Cooling. *Geofluids* **2023**, *2023*, 3819799. [CrossRef]
25. Shao, Z.; Sun, L.; Aboayanah, K.R.; Liu, Q.; Grasselli, G. Investigate the mode i fracture characteristics of granite after heating/-ln2 cooling treatments. *Rock Mech. Rock Eng.* **2022**, *55*, 4477–4496. [CrossRef]
26. Obert, L. *Use of Subaudible Noises for Prediction of Rock Bursts*; US Department of the Interior, Bureau of Mines: Washington, DC, USA, 1941.
27. Goodman, R.E. Subaudible noise during compression of rocks. *Geol. Soc. Am. Bull.* **1963**, *74*, 487–490. [CrossRef]
28. Garg, P.; Zafar, S.; Hedayat, A.; Moradian, O.Z.; Griffiths, D.V. A novel methodology for characterizing fracture process zone evolution in Barre granite specimens under mode I loading. *Theor. Appl. Fract. Mech.* **2023**, *123*, 103727. [CrossRef]
29. Ju, W.; Wang, K. A preliminary study of the present-day in-situ stress state in the Ahe tight gas reservoir, Dibei Gasfield, Kuqa Depression. *Mar. Pet. Geol.* **2018**, *96*, 154–165. [CrossRef]
30. Browning, J.; Meredith, P.G.; Stuart, C.E.; Healy, D.; Harland, S.; Mitchell, T.M. Acoustic characterization of crack damage evolution in sandstone deformed under conventional and true triaxial loading. *J. Geophys. Res. Solid Earth* **2017**, *122*, 4395–4412. [CrossRef]
31. Pestman, B.J.; Van Munster, J.G. An Acoustic Emission Study of Damage Development and Stress-Memory Effects in Sandstone. *Int. J. Rock Mech. Min. Sci. Geomech. Abstr.* **1996**, *33*, 585–593. [CrossRef]
32. Han, J.; Wang, J.; Cheng, C.; Zhang, C.; Liang, E.; Wang, Z.; Song, J.J.; Leem, J. Mechanical response and parametric analysis of a deep excavation structure overlying an existing subway station: A case study of the Beijing subway station expansion. *Front. Earth Sci.* **2023**, *10*, 1079837. [CrossRef]
33. Han, J.; Wang, J.; Jia, D.; Yan, F.; Zhao, Y.; Bai, X.; Yan, N.; Yang, G.; Liu, D. Construction technologies and mechanical effects of the pipe-jacking crossing anchor-cable group in soft stratum. *Front. Earth Sci.* **2023**, *10*, 1019801. [CrossRef]
34. Li, T.L.; Zhao, W.; Liu, R.; Han, J.Y.; Jia, P.J.; Cheng, C. Visualized direct shear test of the interface between gravelly sand and concrete pipe. *Can. Geotech. J.* **2023**. [CrossRef]
35. Gong, L.; Han, D.; Chen, Z.; Wang, D.; Jiao, K.; Zhang, X.; Yu, B. Research status and development trend of key technologies for enhanced geothermal systems. *Nat. Gas Ind. B* **2023**, *10*, 140–164. [CrossRef]

36. Kuruppu, M.D.; Obara, Y.; Ayatollahi, M.R.; Chong, K.P.; Funatsu, T. ISRM-suggested method for determining the mode I static fracture toughness using semi-circular bend specimen. *Rock Mech. Rock Eng.* **2014**, *47*, 267–274. [CrossRef]
37. Hou, P.; Gao, F.; Ju, Y.; Liang, X.; Zhang, Z.; Cheng, H.; Gao, Y. Experimental investigation on the failure and acoustic emission characteristics of shale, sandstone and coal under gas fracturing. *J. Nat. Gas Sci. Eng.* **2016**, *35*, 211–223. [CrossRef]
38. Hardy, H.R. Applications of acoustic emission techniques to rock and rock structures: A state-of-the-art review. *Acoust. Emiss. Geotech. Eng. Pract. STP* **1981**, *750*, 4–92.
39. Zhao, D.; Zhang, S.; Zhao, Y.; Wang, M. Experimental study on damage characteristics of granite under ultrasonic vibration load based on infrared thermography. *Environ. Earth Sci.* **2019**, *78*, 1–12. [CrossRef]
40. Wang, Y.; Yang, R. Study of the dynamic fracture characteristics of coal with a bedding structure based on the NSCB impact test. *Eng. Fract. Mech.* **2017**, *184*, 319–338. [CrossRef]
41. Xue, Y.; Liu, S.; Chai, J.; Liu, J.; Ranjith, P.G.; Cai, C.; Gao, F.; Bai, X. Effect of water-cooling shock on fracture initiation and morphology of high-temperature granite: Application of hydraulic fracturing to enhanced geothermal systems. *Appl. Energy* **2023**, *337*, 120858. [CrossRef]
42. Li, L.C.; Tang, C.A.; Wang, S.Y.; Yu, J. A coupled thermo-hydrologic-mechanical damage model and associated application in a stability analysis on a rock pillar. *Tunn. Undergr. Space Technol.* **2013**, *34*, 38–53. [CrossRef]